J Appl Electrochem (2013) 43:309–321
DOI 10.1007/s10800-012-0487-0

ORIGINAL PAPER

Electrodeposition of bismuth, tellurium, and bismuth telluride thin films from choline chloride–oxalic acid ionic liquid

Camelia Agapescu · Anca Cojocaru · Adina Cotarta · Teodor Visan

Received: 11 July 2012 / Accepted: 1 October 2012 / Published online: 16 October 2012

Abstract This article presents a series of preliminary results regarding the electrodeposition of bismuth, tellurium, and bismuth telluride films at 60 °C from ionic liquids, containing a mixture of choline chloride and oxalic acid (ChCl–OxA). Ten millimolar concentration solutions of $BiCl_3$ and TeO_2 were used as precursors in this supporting electrolyte. Cyclic voltammetry and electrochemical impedance spectroscopy techniques were used to demonstrate the deposition processes on Pt and Cu electrodes. Long-time electrolyses (30–120 min) performed at 60 °C with potential control (between −0.22 and −0.37 V vs. Ag reference electrode) have resulted in films deposited on copper substrate. Film surfaces were studied by scanning electron microscopy and analyzed by energy dispersive X-ray spectroscopy. The results of this study show that ChCl–OxA ionic liquid may be considered as a promising substitute of aqueous baths for Bi, Te or Bi_2Te_3 film plating.

Keywords Electrochemical deposition · Thin films · Bismuth · Tellurium · Bismuth telluride

1 Introduction

The normal procedures used for deposition of thin films, such as evaporation, sputtering, vapor deposition, involve a rather complicated process sequence (heating, vacuum) which is not suitable for industrial applications. In contrast, the electrodeposition is an effective, available method and low cost preparation technique which has been successfully applied to production of semiconductor material films onto electrodes of variable geometry. The operating conditions of electrolysis can be adjusted for thickness, composition (including doping concentration), and morphology control to correlate them with desired properties.

Bismuth is an important chemical element largely used for its unusual electronic, thermoelectrical, and magnetoresistance properties, having as well many applications in electrochromic and piezoelectric devices, electrochemical sensors, catalysis, and superconductivity. Although the recipes for electrodeposition of Bi from aqueous solutions are known since 1933 [1] and there is also information about the kinetics of cathodic process [2–10] as well as underpotential deposition (UPD) [11–13], the reduction of bismuth ions in other media has not been studied extensively. However, there are some papers published in the field of electrochemical behavior of Bi and the mechanism of its electrodeposition in non-aqueous media [14] such as organic media [15–17] or molten salts [18, 19].

Bismuth films with various morphologies and with particle size decreasing from micrometer to nanometer have been successfully prepared by electrodeposition onto metallic or semiconductor electrodes at room temperature. However, the morphology of the deposits is strongly dependent on preparation conditions, such as deposition potential, current density, electrode and electrolyte.

In a recent paper, large dendritic Bi nanostructures have been successfully electrodeposited at room temperature, employing $Bi(NO_3)_3{\cdot}5H_2O$ as Bi precursor without assistance of any additive in aqueous solution and protection of an inert atmosphere [20]. The characterization showed the influences of Bi^{3+} ionic state in the system, the deposition time and of the complexing agents or surfactants on the

C. Agapescu · A. Cojocaru (✉) · A. Cotarta · T. Visan
Department of Inorganic Chemistry, Physical Chemistry and Electrochemistry, University POLITEHNICA of Bucharest, Calea Grivitei 132, 010737 Bucharest, Romania
e-mail: a_cojocaru@chim.upb.ro

formation and morphology of Bi dendrites. Yang [21] developed a procedure of potentiostatic polarization in two steps. In a pre-deposition step, the nucleation and growth of "stagnant" hydrogen bubbles on electrode surface is controlled. Subsequently, in the second step, the simultaneous electrochemical reductions of Bi^{3+} and H^+ ions performed at a constant overpotential lead to Fern-shaped single-crystal bismuth dendrites; thus, the template of hydrogen bubbles limits the lateral growth of Bi dendrites. Recently, Som et al. [22] reported for the first time in literature, a quick and direct single-step fabrication of high-purity Bi hexagonal single crystals under surfactant-free conditions. The Bi precursor $Bi(NO_3)_3{\cdot}5H_2O$ was dissolved (0.5 M) in a 1 M HNO_3 aqueous solution. The authors obtained Bi hexagons by polarizing copper substrate to very high cathodic overpotentials (typically 10 V) far away from the standard reduction potential of Bi^{3+} ion to Bi(0).

Regarding the reversibility of the Bi deposition, it seems that in most cases this is a diffusion controlled and reversible process [7], although there are some authors which proved also its poor reversibility [2] or even a totally irreversible reaction [6].

Tellurium is a semiconductor with energy gap band of 0.4 eV and rather a high electrical conductivity at room temperature; as a consequence, Te electrode behaves as a metallic one in an electrolyte solution. Investigation of Te electrodeposition mechanism and nucleation onto different substrates in aqueous solutions is of great interest because tellurium and telluride films are used for manufacturing of infrared detectors, laser diodes, thermophotovoltaic energy converters or other solar cells, hydrogen generation, electrochemical sensors, thermoelectric power generation, and cooling [23–30]. The kinetics of cathodic reduction of Te-ion was also investigated in organic media [31] or molten salts [19]. By a special procedure, Te-thin films (as well as Bi-thin films) were successfully deposited using the sacrificial Ni-, Co-, or Fe-thin films during galvanic displacement [32]. All authors agree that adsorption and UPD cathodic process are involved in the electrodeposition of elementary tellurium. The low solubility of tellurium oxide or similarly of other precursors in electrolyte solutions explains the diffusion control of the electrodeposition kinetics.

Bismuth telluride belongs to the class of VA–VIA binary chalcogenide compound semiconductor with a narrow energy band gap of 0.13 eV. Two appreciated reviews [33, 34] showed that bismuth telluride, Bi_2Te_3, and its ternary compounds with antimony or selenium are the most widely used thermoelectric materials for room temperature applications. The electrochemical preparation of Bi_2Te_3 semiconductor films has attracted considerable interest because the advantages of electrolysis procedure versus other physical, chemical or metallurgical procedures. There have been a large number of recent published studies concerning Bi_2Te_3 thin and thick films electrodeposition from aqueous electrolytes [35–50], but the majority of these papers concern acidic solutions (with nitric acid, in majority). Electrodeposition from non-aqueous media [51–53] was also reported. The cathodic process implies the presence in the bath of both elements introduced as dissolved precursors, but the weak solubility of bismuth compounds in comparison to tellurium compounds (dioxide, salts, tellurous acid) generally imposes an acidic electrolyte. The recommended baths (1 M HNO_3 solutions) contain generally 1–10 mM concentrations of Bi^{3+} and Te^{4+} (as $HTeO_2^+$) ionic species. The selection of deposition voltage and nature of support were performed usually by cyclic voltammetry tests.

Li et al. [38, 42] have electrodeposited nanostructured bismuth telluride thick films with a thickness up to 350 μm, more suitable for application in thermoelectric devices, from an aqueous solution containing bismuth nitrate and tellurium dioxide in 1 M nitric acid onto gold-sputtered aluminum. The films have a high homogeneity with a stoichiometric composition of Bi_2Te_3. It was shown the beneficial effect of adding ethylene glycol to the electrolyte on the structure, morphology, and compositional stoichiometry of the deposited bismuth telluride films. The films have polycrystalline Bi_2Te_3 hexagonal unit cells with an average crystallite size of around 10–30 nm. The authors suggested that the formation of *n*-type or *p*-type bismuth telluride is related to the microstructure rather than to stoichiometry.

As room temperature ionic liquids were increasingly applied for electrochemical purposes recently, the electroplating of bismuth containing films has been investigated. Earlier, the deposition of a BiSrCaCu superconductor alloy was studied in an ionic liquid based on 1-methyl-3-ethylimidazolium chloride/$AlCl_3$ (EMIC–$AlCl_3$) at 120 °C [54]. Pan and Freyland [55] employed also an acidic chloroaluminated ionic liquid, 1-methyl-3-butylimidazolium chloride–aluminum chloride (MBIC–$AlCl_3$ 42:58 mol %) containing $BiCl_3$, to investigate the electrocrystallization of Bi on Au electrode. In a very recent paper, Fu et al. [56] demonstrated a preliminary adsorption and UPD process of bismuth ions on Au electrode in a 1-butyl-3-methylimidazolium tetrafluoroborate ($BMIBF_4$) ionic liquid. In general, the majority of works on electrodeposition of metals in ionic liquids show that the reduction process in such media is distinct from that in aqueous solutions because of the differences in viscosity, conductivity, potential window, double layer structure, etc.

Abbott et al. [57] have described different types of ionic liquids based on choline chloride (2-hydroxy-ethyl-trimethyl ammonium chloride, ChCl) and their applications. Comparing to other ionic liquids, such media have the additional advantages to be easy to prepare, to be water and air stable and to be cheap, which enables their use in large scale applications. These ionic liquids should be considered

as an attractive alternative to aqueous media for the electrodeposition as they have a low toxicity or they are entirely nontoxic. The greater the thermal stability and the higher the conductivity of the ionic liquid the better the possibility to obtain crystalline semiconductor films through direct electrodeposition at higher temperatures without subsequent annealing.

We recently showed the possibility of electrodeposition of Bi and Te as elements or as binary compound using ionic liquids consisted in eutectic mixtures of choline chloride with urea [58, 59] or with malonic acid [60, 61] as hydrogen bond donors. In this article, we present a preliminary investigation of obtaining Bi, Te, and Bi_2Te_3 thin films from ionic liquid formed mixing choline chloride and oxalic acid (ChCl-OxA). This kind of 1:1 (molar ratio) mixture ionic liquid was first developed by Abbott et al. [62] and consists in a deep eutectic due to hydrogen bonding interactions of choline chloride and oxalic acid. According to our knowledge the deposition process of Bi, Te, and Bi_2Te_3 thin films in ChCl–OxA electrolytes is reported in this article for the first time. In addition, this ionic liquid has potential advantages over other choline-chloride-based ionic liquids related to avoiding the necessity for drying pre-treatment, complexing agents, and grain-refinement additives.

We present the cyclic voltammetry and electrochemical impedance spectroscopy results regarding the electrodeposition and dissolution of films (Bi, Te and Bi_2Te_3) at 60 °C constant temperature. The film preparation and examination of both morphologies and composition of films grown on Cu substrate by long-time electrolysis is also reported.

2 Experimental part

The investigated ionic liquids as background electrolytes were prepared as a mixture (ChCl–OxA 1:1 mol ratio) of choline chloride (99 %) with oxalic acid dihydrate, all reagents being purchased from Aldrich. The appropriate binary mixture was heated at above 90 °C for 30 min until homogeneous colorless ionic liquid is formed. $BiCl_3$ (Aldrich) and TeO_2 (Alfa Aesar) were used as precursors for dissolved ionic species of bismuth and tellurium. The molarities were calculated using density value of 1.2122 g cm^{-3} determined in our laboratory at working temperature.

Cyclic voltammograms (CVs) and electrochemical impedance spectra (EIS) were recorded using a Pt plate (0.5 cm^2) or a Cu disk (0.196 cm^2) as working electrodes to evidence the cathodic and anodic processes in non-stirred aerated baths. Pt plate as auxiliary electrode and Ag wire (immersed in the same ionic liquid) as reference electrode were also used in the electrochemical cell. A SP150 Bio-Logic Sci. Instr. potentiostat was used for both cyclic voltammetry (3-100 mVs^{-1} scan rates) and electrochemical impedance spectroscopy (10 mV a.c. voltage, 200 kHz–50 mHz frequency range).

Bi, Te, and Bi_2Te_3 were deposited on commercial Cu sheets (10–14 cm^2 exposed area) using an increased deposition duration and also a potentiostatic deposition control, at 60 °C constant temperature in aerated baths. The substrate surface was polished before each experiment using emery paper (gradually up to grid 2000), then degreased with acetone, etched for a short time in a HNO_3 solution, rinsed with Milli Q water and dried. After plating the samples were rinsed again with water and dried. A scanning electron microscope QUANTA INSPECT F, working with field emission gun (1.2 nm resolution) and with an energy dispersive spectroscope (EDX, MnK resolution at 133 eV), was used to determine surface morphology and composition of deposited films.

3 Results and discussion

By considering the ChCl–OxA supporting electrolyte with dihydrated oxalic acid ($H_2C_2O_4{\cdot}2H_2O$) used in this article, we mention that the potential window of this electrolyte decreases in the presence of water because the water molecules lead to an easier hydrogen evolution at the electrode surface. However, we consider that the hydration water content provided from oxalic acid does not behave like bulk water, meaning that the water is strongly associated with the chloride anions or with center of possible complex species involving Bi and/or Te.

3.1 Cyclic voltammetry studies

Cyclic voltammetry is used to select potential regions for films electrodeposition, and also for investigating the electrode processes. We mention that no faradaic processes are observed on both Pt and Cu electrodes in the background electrolyte (ChCl–OxA ionic liquid) by polarizing in a wide range of potentials.

Figure 1 shows CVs of deposition and dissolution of 10 mM Bi^{3+} on platinum plate electrode (0.5 cm^2). CV from Fig. 1a presents the current–potential relation recorded in the a large potential range, from −1 to +1.2 V; it has only a single pair of peaks, the anodic one being more prominent due to dissolution of a significant amount of bismuth deposit. The family of CVs restricted to the Bi deposition/dissolution region in the same ionic liquid is shown in Fig. 1b. It may be observed that starting from +0.05 V a less observed process occurs, which may be assigned to UPD of Bi on platinum. The onset of bulk deposition of bismuth at −0.1 V may be noticed for all scan rates, followed by well-defined reduction peaks within

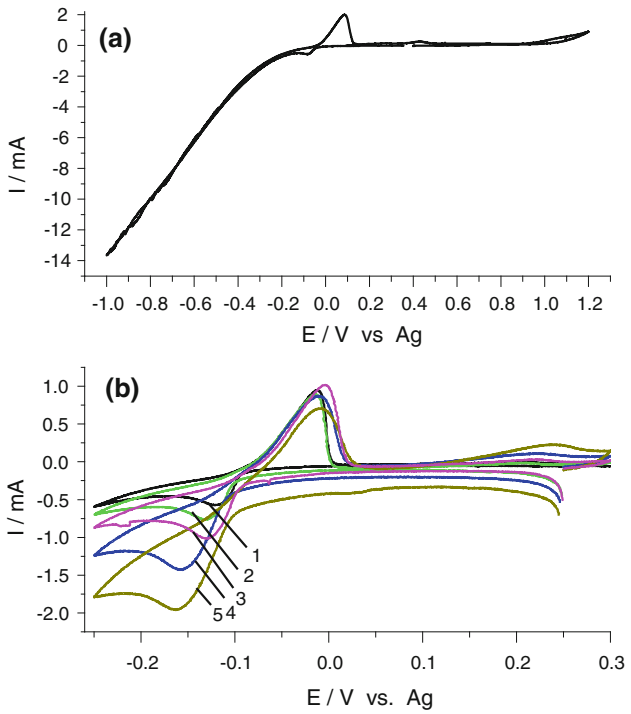

Fig. 1 CVs on Pt from ChCl–OxA + 10 mM $BiCl_3$ ionic liquid at 60 °C. **a** CV recorded within large potential range, scan rate 20 mVs^{-1}; **b** CVs with scan rates: (*1*) 5 mVs^{-1}; (*2*) 10 mVs^{-1}; (*3*) 20 mVs^{-1}; (*4*) 50 mVs^{-1}; (*5*) 100 mVs^{-1}

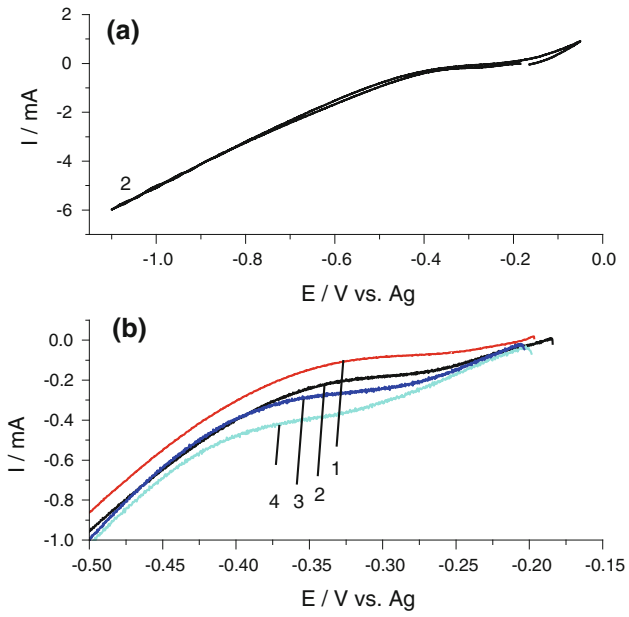

Fig. 2 CVs on Cu from ChCl–OxA + 10 mM $BiCl_3$ ionic liquid at 60 °C. **a** CV curve 2 is recorded within large cathodic potential range, scan rate 20 mVs^{-1}; **b** portions of cathodic branches of CVs with scan rates: (*1*) 5 mVs^{-1}; (*2*) 20 mVs^{-1}; (*3*) 50 mVs^{-1}; (*4*) 100 mVs^{-1}

the potential range from −0.12 to −0.17 V. Scanning the potential toward more negative values results in a continuous increase of current that may be a continuation of Bi deposition together with hydrogen evolution. A quantitative interpretation of CVs may lead to the conclusion that it appears to be a linear dependence of cathodic peak current with the square root of scan rate that may indicate a diffusion control for kinetics of reduction process. Although reversible cathodic process should be expected for this simple process $Bi^{3+} \rightarrow Bi^0$, the shift with scan rate of cathodic peak potential toward more negative potentials and values of peak potential separation (ΔE_p) of 100–170 mV prove a rather quasireversible reduction in this medium, more viscous than conventional solutions.

CVs in Fig. 1b show that, during potential scan in positive direction, an anodic peak at about −0.02 V potential occurs, this main peak corresponding to stripping of deposited bismuth; its peak current does not vary linearly with scan rate. Moreover, a supplementary wave located at +0.23 V is visible especially at higher scan rates, which may be assigned to the dissolution of UPD Bi layer, first formed on platinum.

CVs of Bi using copper disk electrode of 0.196 cm^2 surface area (Fig. 2) have a different shape than for platinum electrode. They exhibit a cathodic plateau of limiting currents which start within the potential range from −0.25 to −0.32 V, depending on the scan rate. At more negative polarization, for instance up to −1.1 V for curve 2 in Fig. 2a, one may notice only a continuous increase of current. This last cathodic part represents simultaneous competing reactions of the discharge of Bi^{3+} and hydrogen evolution. Returning the potential in the anodic direction, we stopped the scan at around 0 V potential, to avoid the dissolution of copper substrate that certainly may occur together to dissolution of bismuth film.

The values of cathodic limiting current increase with scan rate, so it is possible for Bi deposition on copper to be also a diffusion controlled process. In comparison with CVs on Pt, the current densities are of the same order of magnitude exhibiting a similar kinetics of deposition.

Similar interpretation of processes can be made for tellurium ion behavior on Pt and Cu electrodes. Regarding the voltammograms on platinum, Fig. 3a presents a single CV (curve 4) recorded on a large potential range showing also a single pair of peaks. Along cathodic branches of CVs from Fig. 3b it may observe first the process of UPD of tellurium within potential range from +0.5 to +0.35 V and a single well-defined cathodic peak at around +0.3 V for lowest scan rates; the peak potential has a gradual shift toward negative direction with higher scan rates. The current increase at the end of cathodic scan is attributed to hydrogen evolution that occurs at potentials more negative than −0.3 V. On the anodic branches of CVs, the main oxidation process is represented by a well-defined peak

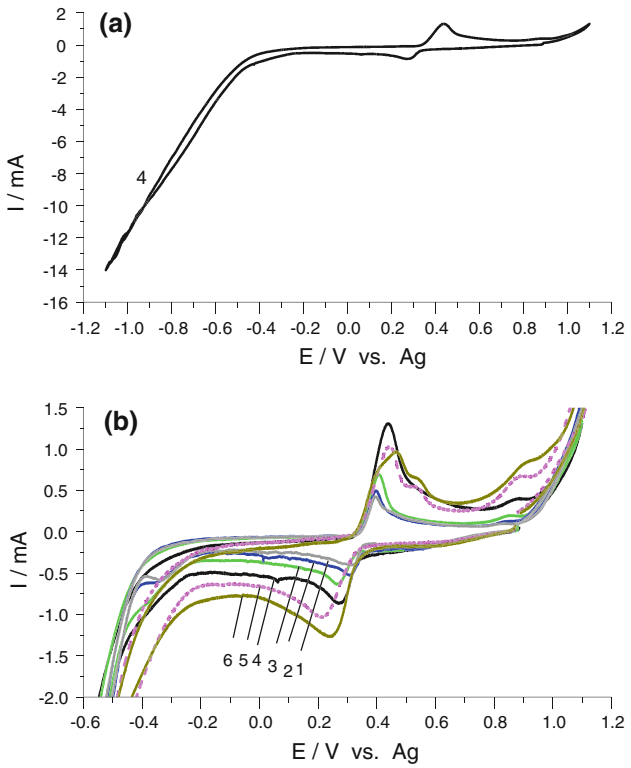

Fig. 3 CVs on Pt from ChCl–OxA + 10 mM TeO_2 ionic liquid at 60 °C. **a** CV curve 4 is recorded within large cathodic potential range, scan rate 20 mVs^{-1}; **b** portions of CVs with scan rates: (*1*) 3 mVs^{-1}; (*2*) 5 mVs^{-1}; (*3*) 10 mVs^{-1}; (*4*) 20 mVs^{-1}; (*5*) 50 mVs^{-1}; (*6*) 100 mVs^{-1}

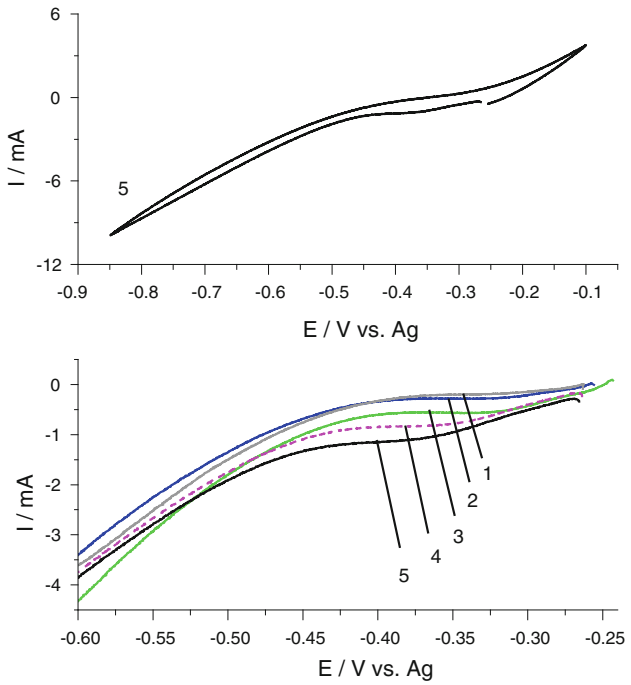

Fig. 4 CVs on Cu from ChCl–OxA + 10 mM TeO_2 ionic liquid at 60 °C. **a** CV recorded within large cathodic potential range, scan rate 100 mVs^{-1}; **b** portions of cathodic branches of CVs with scan rates: (*1*) 3 mVs^{-1}; (*2*) 5 mVs^{-1}; (*3*) 10 mVs^{-1}; (*4*) 20 mVs^{-1}; (*5*) 50 mVs^{-1}; (*6*) 100 mVs^{-1}

located at around +0.45 V showing dissolution of deposited tellurium. The potential of this peak remains almost constant with scan rate, although the peak potential separation ΔE_p increases with scan rate from 80 to 150 mV. An additional wave, less visible at slow scan rate, is noticed near the anodic peak that is probable due to stripping of Te deposited by UPD. The third process occurring at the end of anodic branches is a well-defined wave located at +0.9 V that may represent an oxidation process of a component from supporting electrolyte, most probably the oxidation of free Cl^- ions from choline chloride.

More simple processes are exhibited by Fig. 4 regarding behavior of Te^{4+} ion using disk copper electrode. Here, the cathodic branches of all CVs show clearly the onset of reduction process $Te^{4+} \rightarrow Te^0$ at −0.245 V followed by limiting current plateau reached at potentials from −0.32 to −0.35 V. UPD processes of Te on Cu are visible only at very slow scan rates (3 or 5 mVs^{-1}). Polarization at more negative potentials than −0.42 V leads to a continuous increase of current which is mainly due to the hydrogen evolution, as was mentioned above.

However, a comparison with Fig. 2 shows that the cathodic process of Te^{4+} proceeds on Cu at more negative potentials than for reduction of Bi^{3+}, hence in fact is an inverse order of reduction on Pt than on Cu substrate. Therefore, the nature of support is found to have a marked influence on the reduction potentials of bismuth and tellurium.

Typical CVs recorded at Pt for the system containing both Bi^{3+} and Te^{4+} ions in ChCl–OxA ionic liquid at 60 °C are shown in Fig. 5. On the cathodic scan, we found out a series of consecutive processes represented first by a broad peak in the most positive region, then by two waves and finally by the continuous increase of current. According to the electrode potentials of processes exhibited on previous CV experiments with single ions, we attribute the first process to UPD of tellurium (potentials from +0.5 to +0.1 V). More negatively, a bulk co-deposition of Bi and Te producing a Bi_2Te_3 containing film may be illustrated as a current wave in the range between +0.1 and −0.1 V. The co-deposition process may be described by the following reactions involving either Te^{4+} ion [48] or $HTeO_2^+$ ion [33], (this ionic species is usually present in water containing media):

$$xBi^{3+} + yTe^{4+} + (3x + 4y)e^- \rightarrow Bi_xTe_y \quad (1)$$

$$xBi^{3+} + yHTeO_2^+ + 3yH^+ + (3x + 4y)e^- \rightarrow Bi_xTe_y + 2yH_2O \quad (2)$$

By a more negative scanning, the limiting current wave of Bi_2Te_3 co-deposition is followed by a new wave with

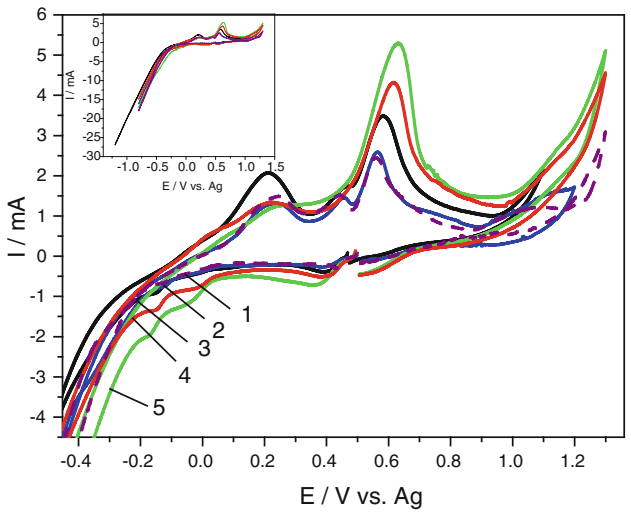

Fig. 5 CVs on Pt from ChCl–OxA + 10 mM $BiCl_3$ + 10 mM TeO_2 ionic liquid at 60 °C. Scan rates (*1*) 5 mVs^{-1}; (*2*) 10 mVs^{-1}; (*3*) 20 mVs^{-1}; (*4*) 50 mVs^{-1}; (*5*) 100 mVs^{-1}. Cathodic potential limits were shown in insertion

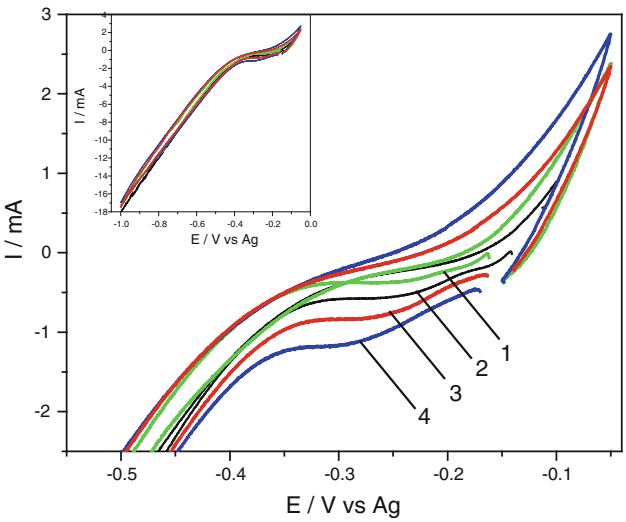

Fig. 6 CVs on Cu from ChCl–OxA + 10 mM $BiCl_3$ + 10 mM TeO_2 ionic liquid at 60 °C. Scan rates (*1*) 10 mVs^{-1}; (*2*) 20 mVs^{-1}; (*3*) 50 mVs^{-1}; (*4*) 100 mVs^{-1}. Cathodic potential limits were shown in insertion, where all CVs are overlapped

increasing current attributed to a process involving a supplementary Bi deposition together Bi_2Te_3 deposition; this wave starts at −0.1 V and ends to −0.2 V. Within the straight potential range the rate of Bi_2Te_3 co-deposition may be slow, so excess Bi inclusion can be expected to be in the deposit. This Bi-enriching process may have a great technological importance for an appropriate selection of potentials to obtain Bi_2Te_3 containing films with desired composition. Of course, the final part on the cathodic polarization is hydrogen evolution, as discussed above.

The interpretation of anodic branch of CVs in Fig. 5 is related to the oxidation processes in an exactly reverse sequence as reduction processes. Thus, first anodic peak located at +0.2 V represents Bi dissolution. The second oxidation process corresponds to Bi_2Te_3 dissolution and the third to dissolution of UPD Te layers. However, these processes are visible separately only at slow scan rates (peaks at +0.42 and +0.57 V). Because the peak potential of Bi_2Te_3 dissolution shifts significantly toward positive direction at higher scan rates, both processes are overlapped as a single peak with peak potentials from +0.57 to +0.61 V. Finally, the current increase at more positive potentials than +1.1 V is due to the oxidation processes of supporting electrolyte (ChCl–OxA), probably of free Cl^- ions.

In the same manner we can interpret the processes during the cathodic polarization of disk Cu electrode in the same system containing both Bi^{3+} and Te^{4+} ions. As Fig. 6 shows, on the cathodic branches of CVs the first process of UPD (Bi and Te) is almost absent being evidenced only at relatively slow scan rates (portions of curves 1 and 2 at potentials between −0.17 and −0.2 V). The limiting currents along the main plateau within the potential range from −0.2 to −0.35 V are associated with the Bi and Te co-deposition. The existence of this process is confirmed by SEM and EDX measurements for Bi_2Te_3 containing films prepared on Cu support, as we will discuss in the last part of the paper. It is obvious from Fig. 6 that the limiting current increases with scan rate suggesting also a diffusion control of co-reduction process on copper, similarly as on platinum. In the final part of the cathodic scan performed up to −1 V a competition of Bi and Bi_2Te_3 deposition on a hand with hydrogen evolution on the other hand may be possible. This is confirmed by a decreased faradaic efficiency from technological point of view.

As an overall consideration, it is worth to note that the anodic curves for this system are similar for all CVs recorded on Cu electrode (Figs. 2, 4, 6).

3.2 EIS measurements

We present in this part Nyquist diagrams (imaginary part of impedance vs real part) and Bode diagrams (both dependences with frequency of phase angle and impedance modulus) obtained experimentally by shifting negatively the electrode potential from stationary potential. We have used the CVs to select the appropriate potentials for polarization, therefore the sequences presented here should be interpreted similarly that CV results. Figure 7 presents EIS curves for Bi deposition on Pt (0.5 cm^2). Nyquist spectra from Fig. 7a show clearly a single semicircle at stationary potential; by gradual cathodic polarization, this capacitive loop is continued at low frequencies with a

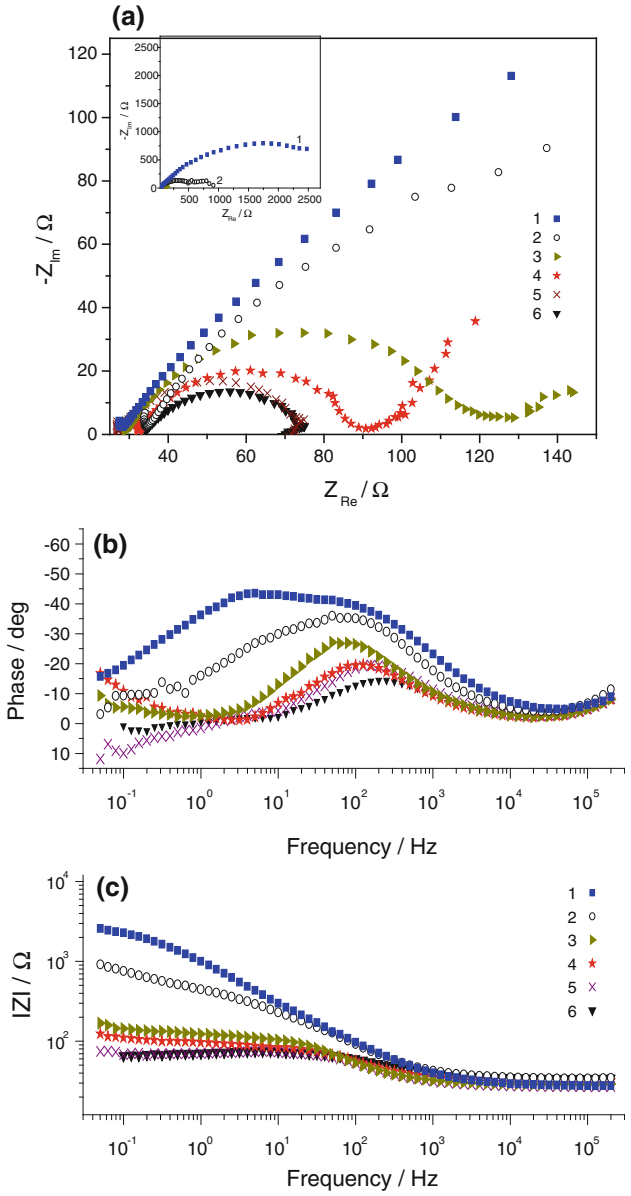

Fig. 7 EIS spectra on Pt from ChCl–OxA + 10 mM $BiCl_3$ ionic liquid at 60 °C. Different polarization potentials starting from $E_{stationary} = +0.2$ V (vs. Ag ref.): (*1*) +0.2; (*2*) +0.1; (*3*) 0; (*4*) −0.2; (*5*) −0.3; (*6*) −0.4 V; **a** Nyquist plots, including portions at high impedances in insertion; **b**, **c** Bode plots

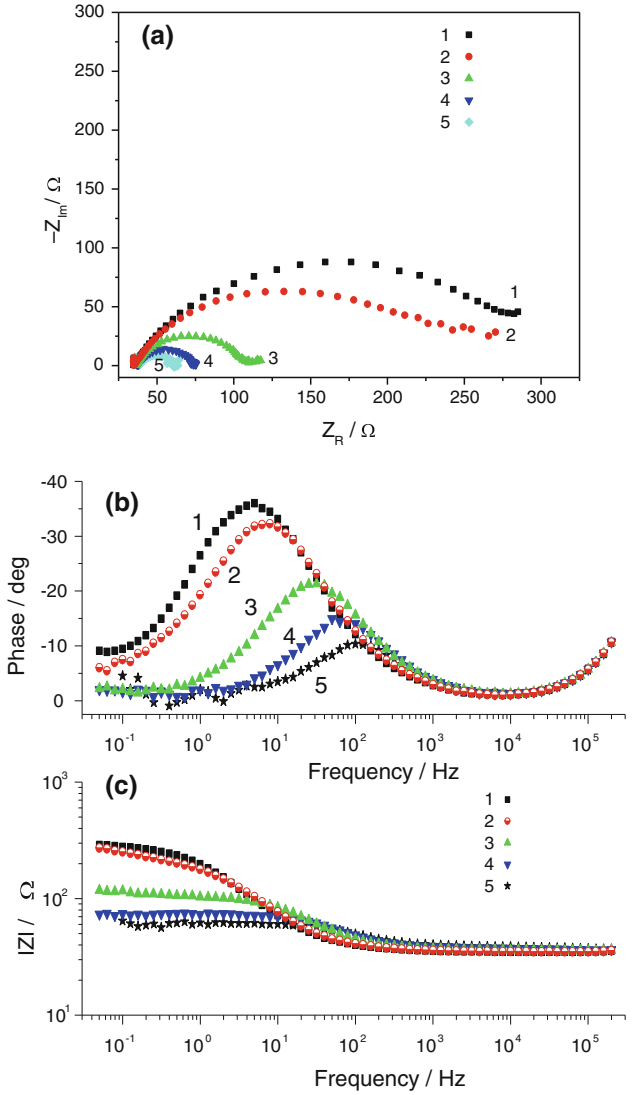

Fig. 8 EIS spectra on Cu from ChCl–OxA + 10 mM $BiCl_3$ ionic liquid at 60 °C: **a** Nyquist plots; **b**, **c** Bode plots. Different polarization potentials starting from $E_{stationary} = -0.168$ V (vs. Ag ref.): (*1*) −0.17; (*2*) −0.27; (*3*) −0.37; (*4*) −0.47; (*5*) −0.57 V

linear portion with slope approaching one, attributed to diffusion within thin film deposited on electrode.

It can be seen in Fig. 7a that polarization from +0.2 V (stationary potential) to −0.4 V results in a sequence of decreased diameters of capacitive semicircles. The diameters correspond to charge-transfer resistances, R_{ct}, with values decreasing from 11,500 Ω cm^2 up to 25 Ω cm^2. Correspondingly, the maximum of Bode angle (Fig. 7b) decreases gradually from −45° to −14°, this last value being attributed to a metallic behavior of Bi deposit. Dependences of impedance modulus with frequency (Fig. 7c) present also a gradual decrease, confirming the continuous deposition process of bismuth that behaves as a metal (Fig. 8).

The comments regarding EIS spectra for all the other cases (Bi deposition on Cu, Te deposition on Pt and Cu, as well as Bi_2Te_3 deposition on Pt and Cu) reveal similar aspects, proving an increased evolution of faradaic process by shifting the potential more negatively. In some cases (Figs. 9, 11, 12) depressed/distorted semicircles are observed, a fact that may be due to non-uniformity of support surface or rugosity of deposit. Also, in some working conditions the sequence of EIS curves is not in order of applied potentials (see Figs. 9, 10, 11) mostly owing to the quasi-capacitive properties of film deposited first on the substrate surface. It is interesting to note that the distinct presence of

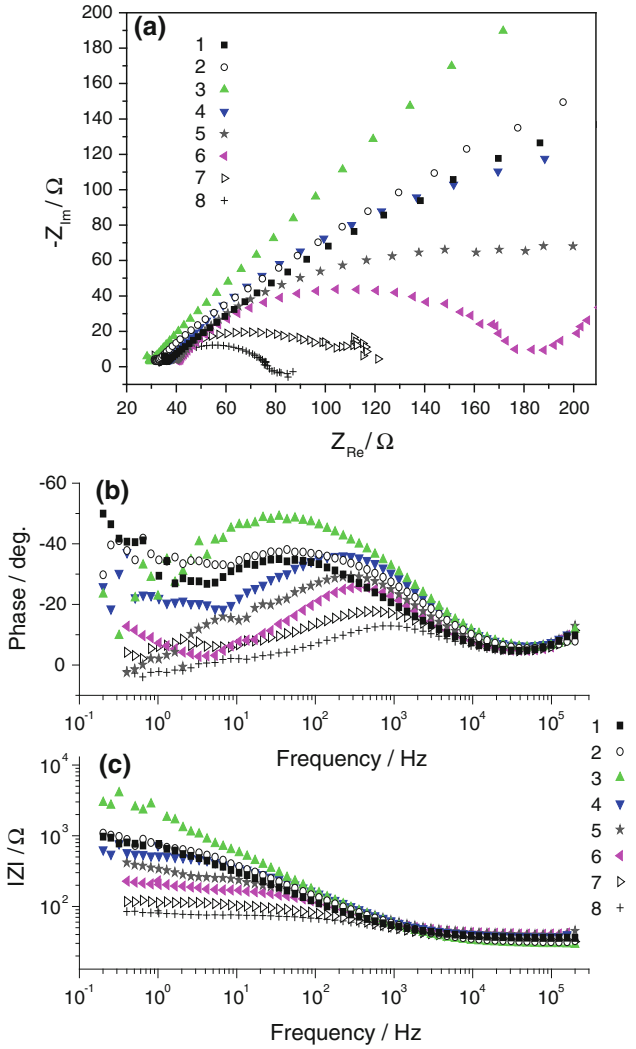

Fig. 9 EIS spectra on Pt from ChCl–OxA + 10 mM TeO_2 ionic liquid at 60 °C: **a** Nyquist plots; **b**, **c** Bode plots. Different polarization potentials starting from $E_{stationary} = +0.462$ V (vs. Ag ref.): (*1*) +0.25; (*2*) +0.20; (*3*) +0.05; (*4*) −0.15; (*5*) −0.25; (*6*) −0.35; (*7*) −0.45; (*8*) −0.55 V

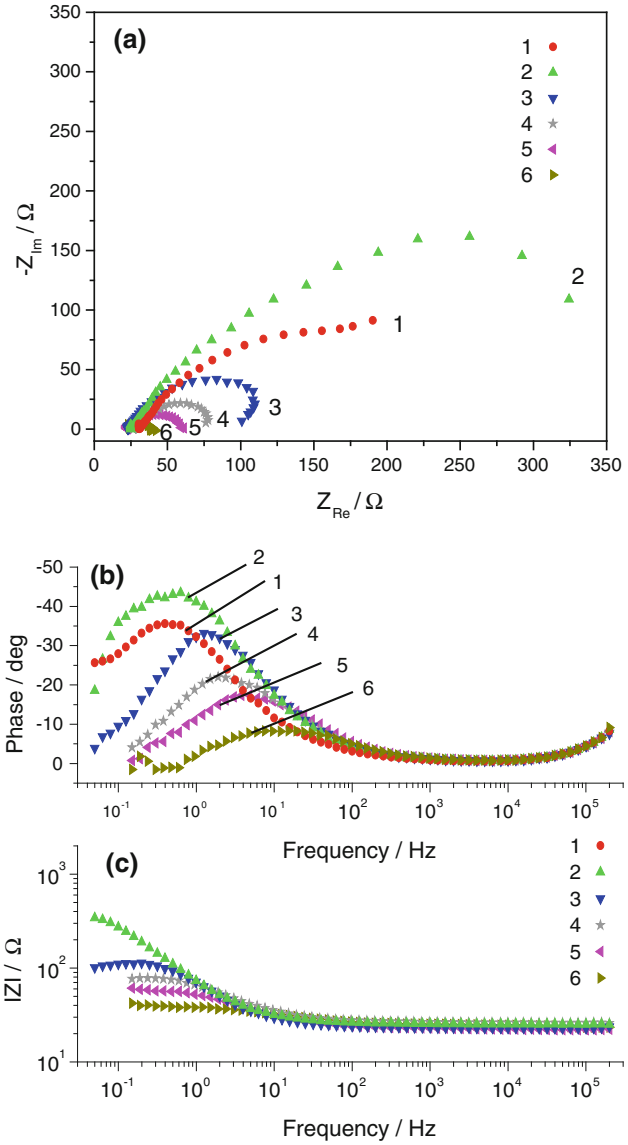

Fig. 10 EIS spectra on Cu from ChCl–OxA + 10 mM TeO_2 ionic liquid at 60 °C: **a** Nyquist plots; **b**, **c** Bode plots. Different polarization potentials starting from $E_{stationary} = -0.245$ V (vs. Ag ref.): (*1*) −0.26; (*2*) −0.30; (*3*) −0.35; (*4*) −0.40; (*5*) −0.45; (*6*) −0.50 V

co-deposition process to form Bi_2Te_3 film together with UPD process is illustrated by two consecutive semicircles (also two phase angle maxima) occurred at +0.4 V polarization in Fig. 11 and at −0.25 V polarization in Fig. 12. In general, we conclude that all EIS results are in a good agreement with the results of CV investigations.

3.3 Preparation and characterization of BiTe-thin films deposited on Cu support

3.3.1 Preparation of film samples

Bi, Te, and Bi_2Te_3 containing thin films were prepared under potentiostatic control on copper sheets from ionic liquids containing choline chloride with oxalic acid mixture. Temperature was maintained constant, at 60 °C. The copper electrodes having a surface area of 9–14 cm^2 were placed vertically to avoid the occlusion of the hydrogen bubbles formed during deposition and to promote natural convection. Long-time electrolyses (30–120 min) were performed by shifting the potential from stationary potential (open-circuit potential OCP) to values ranging from −0.22 to −0.37 V versus Ag reference electrode. Table 1 presents the operating conditions in all baths utilized.

In order to get information about film surface, measurements of the morphological properties and chemical

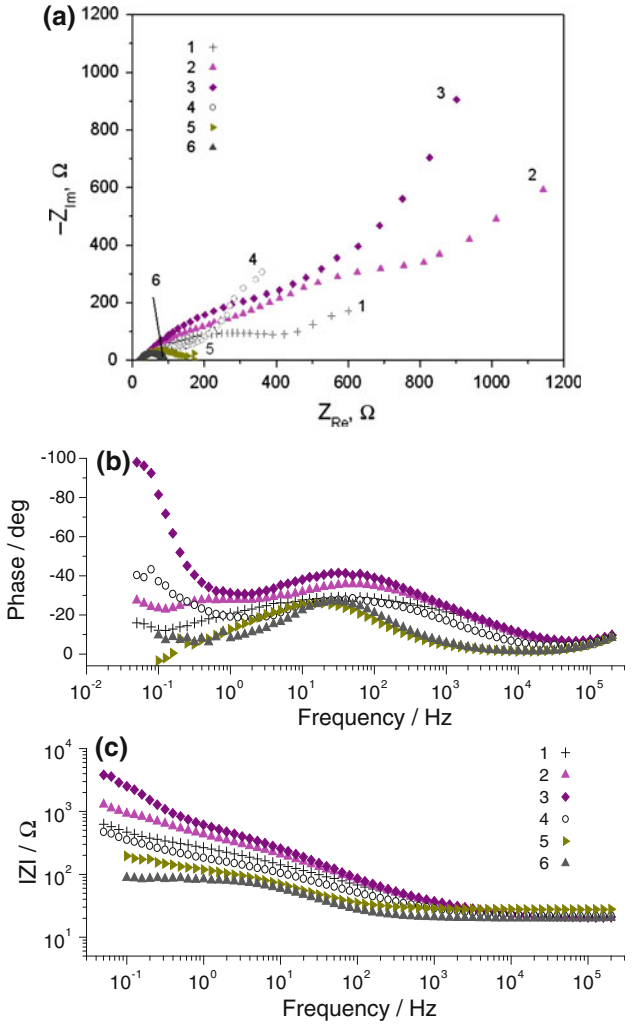

Fig. 11 EIS spectra on Pt from ChCl–OxA + 10 mM $BiCl_3$ + 10 mM TeO_2 ionic liquid at 60 °C: **a** Nyquist plots; **b**, **c** Bode plots. Different polarization potentials starting from $E_{stationary}$ = +0.463 V (vs. Ag ref.): (*1*) +0.43; (*2*) +0.40; (*3*) +0.20; (*4*) 0; (*5*) −0.15; (*6*) −0.25 V

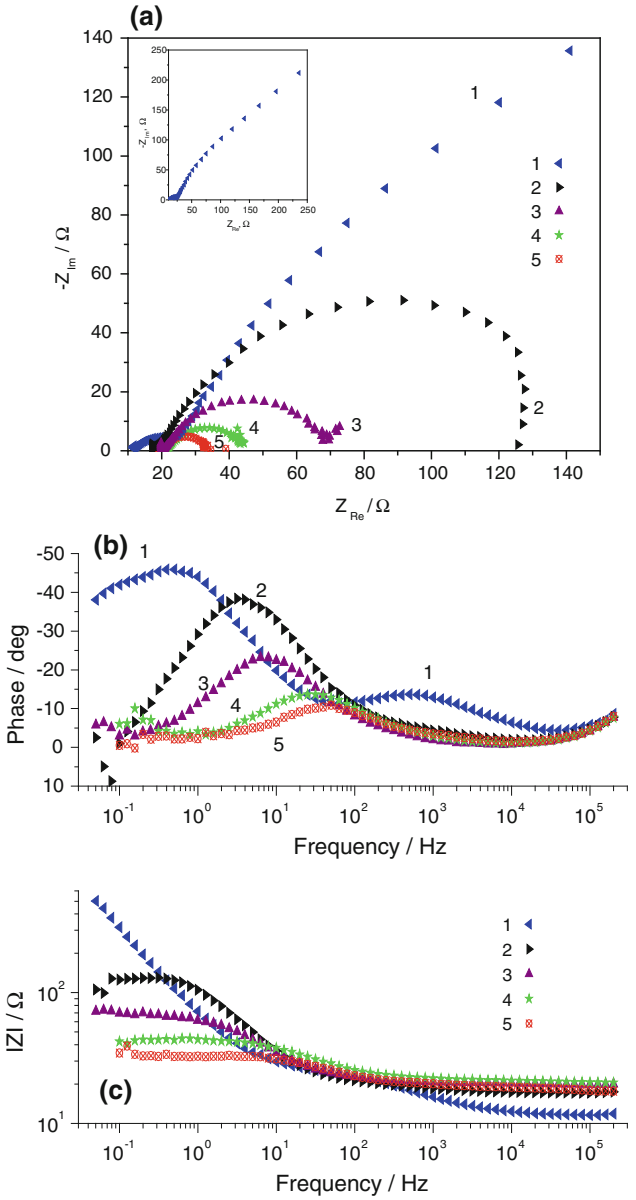

Fig. 12 EIS spectra on Cu from ChCl–OxA + 10 mM $BiCl_3$ + 10 mM TeO_2 ionic liquid at 60 °C: **a** Nyquist plots; **b**, **c** Bode plots. Different polarization potentials starting from $E_{stationary}$ = −0.167 V (vs. Ag ref.): (*1*) −0.25; (*2*) −0.35; (*3*) −0.40; (*4*) −0.50; (*5*) −0.55 V

composition of films deposited on copper substrate were carried out. We present here the results of SEM microscopy and EDX chemical analysis for evaluation of as-deposited films obtained with potentiostatic control. The coatings were as thick as 1–2 μm, and there was no indication that it is not possible to realize even much thicker coatings.

3.3.2 *Morphological study*

Figures 13, 14 and 15 show that different morphologies are obtained for Bi, Te, and Bi_2Te_3 containing films and also there are differences when modifying the applied potential. Figure 13a corresponds to the Bi-1 sample that electrodeposited at −0.220 V for 60 min. It can be seen that the polygonal microcrystals were randomly distributed over the surface, with average particle sizes of 60–90 nm; in few cases they are agglomerated in prismatic shape with 200–400 nm dimensions. Figure 13b exhibits the morphology of Bi-2 sample which electrodeposited at more negative potential (−0.286 V, ca 120 mV overpotential). In this SEM image the polygonal microcrystals, of similar size as previously (60–100 nm as an average), were densely and distributed over the surface as irregular aggregates, with obvious film thickening for longer duration of electrolysis (90 min). These results indicated that the Bi electrodeposits showed 3D morphological characteristics [10] meaning that the aggregated nuclei turned to be denser

Table 1 Electrolysis conditions during preparation of Bi, Te, and Bi_2Te_3 films on copper using ChCl–OxA (1:1) ionic liquid, temperature 60 °C

Film sample	Content of Bi or/and Te precursors in the bath	Stationary potential (OCP) (V vs. Ag ref.)	Controlled potential (V vs. Ag ref.)	Electrolysis time (min)
Bi-1	10 mM $BiCl_3$	−0.168	−0.220	60
Bi-2	10 mM $BiCl_3$	−0.168	−0.286	90
Te-1	10 mM TeO_2	−0.245	−0.298	120
Te-2	10 mM TeO_2	−0.245	−0.370	30
Bi_2Te_3	10 mM $BiCl_3$ + 10 mM TeO_2	−0.167	−0.250	90

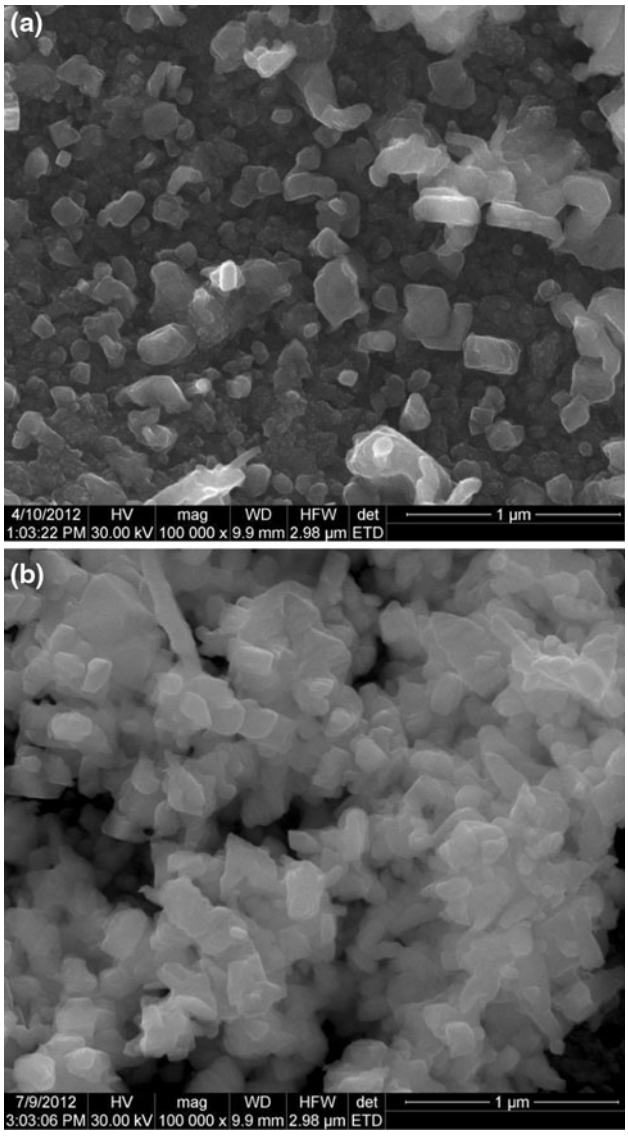

Fig. 13 SEM images of Bi-films deposited on Cu from ChCl–Ox.Ac + 10 mM $BiCl_3$ bath at 60 °C (see deposition conditions in Table 1): **a** Bi-1 film; **b** Bi-2 film. Magnification: ×100,000

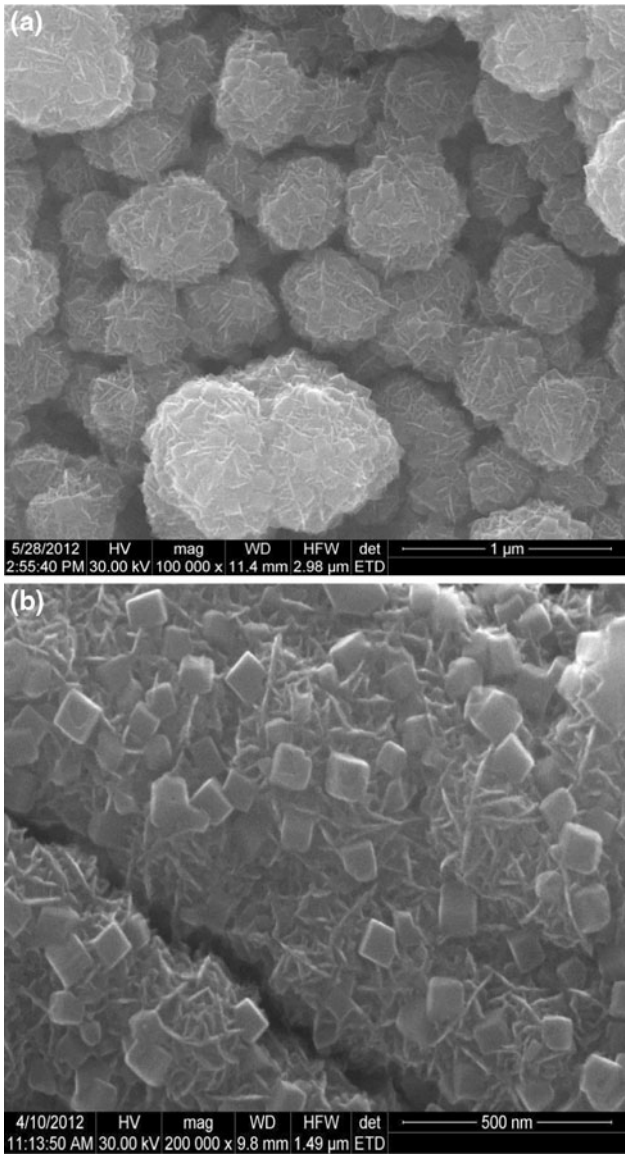

Fig. 14 SEM images of Te-films deposited on Cu from ChCl–Ox.Ac + 10 mM TeO_2 bath at 60 °C (see deposition conditions in Table 1): **a** Te-1 film, magnification: ×100,000; **b** Te-2 film, magnification: ×200,000

when both the deposition overpotential and time increased, thus increasing the uniformity of coating.

From Fig. 14a, b it may be seen that the films electrodeposited from tellurium ion containing electrolyte have a morphology with rather cubic microcrystals. Comparing Te-1 and Te-2 samples, a coarse-grained deposit is for Te-1 film (Fig. 14a) grown at a lower cathodic overpotential (53 mV), but in longer time duration. SEM image of this film evidences microcrystals joined in a spheroidal aggregates in a dense arrangement on the surface. However, more compacted portions with decreasing grain size were for Te-2 film (Fig. 14b) deposited at higher overpotentials (125 mV). The microcrystals for both cases are in close

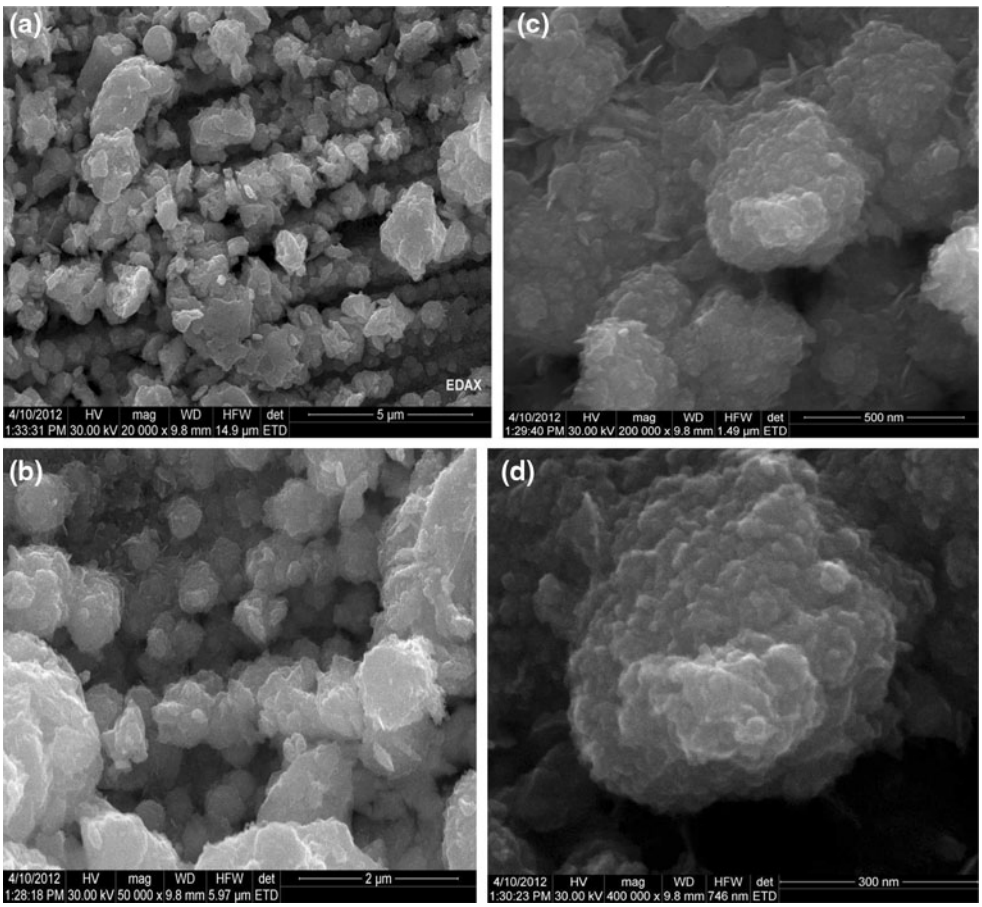

Fig. 15 SEM images of Bi_2Te_3 containing film deposited on Cu from ChCl–Ox.Ac + 10 mM $BiCl_3$ + 10 mM TeO_2 bath at 60 °C (see deposition conditions in Table 1). Gradual magnification: **a** ×20,000; **b** ×50,000; **c** ×200,000; **d** ×400,000

dimensions (60–90 nm as an average). For a good description of morphology of Bi_2Te_3 containing films, we present in Fig. 15 a sequence of SEM micrographs with gradual magnification. The bath containing both bismuth and tellurium ions produced a "cauliflower" type of morphology. Thus, the deposit consisted in nodular aggregates with average dimensions of 200–300 nm and distributed non-homogeneously over the entire surface (Fig. 15a, b). From Fig. 15c, d we can distinguish joined microcrystals having round corners and similar size (10–15 nm as an average). This morphology for thin Bi_2Te_3 films may be attributed to the fast growth of grains with several orientations [63]. As a conclusion, this morphology of Bi_2Te_3 film clearly differs than those for Bi or Te films.

3.3.3 Chemical composition of thin films

Energy dispersive X-ray spectroscopy (EDX) is used as a preliminary diagnostic tool to confirm the formation of Bi, Te, or BiTe on the support surface. The composition data are summarized in Table 2.

Table 2 EDX chemical analysis data for thin films deposited on copper using ChCl–OxA (1:1) ionic liquid

Constituent element	Bi-2 film		Te-1 film		Bi_2Te_3 film	
	wt%	at.%	wt%	at.%	wt%	at.%
Bi L	84.73	29.82	–	–	63.40	33.63
Te L	–	–	84.50	40.58	30.90	26.82
O K	15.27	70.18	15.50	59.42	5.70	39.55

The EDX analyses revealed that for both film samples with singular element (bismuth or tellurium) the content of element was higher than 84 wt%. Oxygen contamination, with similar values (∼15 %) for Bi and Te films, occurs because one has not made use of a glove box and due to the fact that the existence of oxide impurities on the surface before and after deposition may strongly affect the outcome of the analysis. The data for film containing both Bi and Te indicate a composition roughly 2:1 for Bi:Te as weight percentage and roughly 1:1 Bi:Te as stoichiometric ratio. This is a good confirmation of successfully obtaining of a Bi_2Te_3 film having almost the same composition with

the bath (10 mM Bi^{3+} + 10 mM Te^{4+}). Also we can interpret the EDX results as no preferential deposition of either bismuth or tellurium in using ionic liquids containing choline chloride and oxalic acid.

4 Conclusions

In this preliminary study, ChCl–OxA ionic liquid was successfully used as a supporting electrolyte for electrodeposition of Bi or/and Te. Cyclic voltammetry and electrochemical impedance spectroscopy allowed a comparative investigation of cathodic processes on Pt and Cu. Both techniques indicate potentials where films are deposited first as UPD processes and then (at more negative potentials) as bulk deposition. Deposition of a Bi-rich Bi_2Te_3 film associated with hydrogen evolution are expected for higher cathodic overpotentials. SEM images for Bi, Te, and bismuth telluride containing films prepared on Cu plates in potentiostatic conditions showed differences in their morphology due to differences in nucleation and aggregation of microcrystals. Almost 85 wt% purity of Bi and Te films and a stoichiometric 1:1 ratio of Bi:Te in bismuth telluride containing films were confirmed by EDX.

The results of this study show that ChCl–OxA ionic liquid may be considered as a promising substitute of aqueous baths for Bi, Te or Bi_2Te_3 film plating.

Acknowledgments The support of the European Social Fund through POSDRU/88/1.5/S/60203 Project is acknowledged by the first author.

References

1. Harbough M, Mathers FE (1933) Trans Electrochem Soc 64:293
2. Jeffrey CA, Harrington DA, Morin S (2002) Surf Sci 512:L367
3. Jiang S, Huang Y-H, Luo F, Du N, Yan C-H (2003) Inorg Chem Commun 6:781
4. Vereecken PM, Rodbell K, Ji CX, Searson PC (2005) Appl Phys Lett 86:121916
5. Yang M, Hu Z (2005) J Electroanal Chem 583:46
6. Valsiunas I, Miecinskas P, Gudaviciute L, Steponavicius A (2006) Chemija 17(4):35
7. Sandnes E, Williams ME, Bertocci U, Vaudin MD, Stafford GR (2007) Electrochim Acta 52:6221
8. Hocevar SB, Daniele S, Bragato C, Ogorevic B (2007) Electrochim Acta 53:555
9. Holvoet S, Horny P, Turgeon S, Chevallier P, Pireaux J–J, Mantovani D (2010) Electrochim Acta 55:1042
10. Zhou L, Dai Y, Zhang H, Jia Y, Zhang J, Li C (2012) Bull Korean Chem Soc 33(5):1541
11. Hamm UW, Kramer D, Zhai RS, Kolb DM (1998) Electrochim Acta 43:2969
12. Steponavicius A, Gudaviciute L, Karpaviciene V, Kapocius V (2003) Chemija 12(1):42
13. Hara M, Nagahara Y, Inukai J, Yoshimoto S, Itaya K (2006) Electrochim Acta 51:2327
14. Simka W, Puszczyk D, Nawrat G (2009) Electrochim Acta 54:5307
15. Petrova TP, Zelenetskaya KV, Rakhmatullina IF, Shapnik MS (2006) Prot Met 42:359
16. Perelygin YP, Kireev SY, Kireev AY (2006) Russ J Appl Chem 79(7):1200
17. Tsai Y-D, Lien C-H, Hu C-C (2011) Electrochim Acta 56:7615
18. Colom F, Alonso L (1965) Electrochim Acta 10(8):835
19. Ebe H, Ueda M, Ohtsuka T (2007) Electrochim Acta 53:100
20. Ni Y, Zhang Y, Zhang L, Hong J (2011) Cryst Eng Commun 13:794
21. Yang M (2011) J Mater Chem 21:3119
22. Som T, Simo A, Fenger R, Troppenz GV, Bansen R, Pfander N, Emmerling F, Rappich J, Boeck T, Rademann K (2012) Chem Phys Chem. doi:10.1002/cphc.201101009
23. Montiel-Santillan T, Solorza-Feria O, Sanchez-Soriano H (2002) Int J Hydr Energy 27:461
24. Santos MC, Machado SAS (2005) Electrochim Acta 50(11):2289
25. Zhu W, Yang JY, Zhou DX, Bao SQ, Fan XA, Duan XK (2007) Electrochim Acta 52(11):3660
26. Ivanova YA, Ivanov DK, Streltsov EA (2007) Electrochim Acta 52(16):5213
27. Sadeghi M, Dastan M, Ensaf MR, Tehrani AA, Tenreiro C, Avila M (2008) Appl Radiat Isot 66(10):1281
28. She G, Shi W, Zhang X, Wong T, Cai Y, Wang N (2009) Cryst Growth Des 9:663
29. Li F-H, Wang W (2010) J Appl Electrochem 40:2005
30. Santos MC, Cabral MF, Machado SAS (2011) Electrochim Acta 58:1
31. Liftman Y, Albeck M, Goldschmidt JME, Yarnitsky Ch (1984) Electrochim Acta 29:1673
32. Chang CH, Rheem Y, Choa Y-H, Shin DH, Park D-Y, Myung NV (2010) Electrochim Acta 55:743
33. Xiao F, Hangarter C, Yoo B, Rheem Y, Lee K-H, Myung NV (2008) Electrochim Acta 53:8103
34. Boulanger C (2010) J Electron Mater 39:1818
35. Zhu W, Yang JY, Gao XH, Bao SQ, Fan XA, Zhang TJ, Cui K (2005) Electrochim Acta 50(20):4041
36. Yoo BY, Huang C-K, Lim JR, Herman J, Ryan MA, Fleurial J-P, Myung NV (2005) Electrochim Acta 50:4371
37. Wen S, Corderman RR, Seker F, Zhang AP, Denault L, Blohm ML (2006) J Electrochem Soc 153:C595
38. Li S, Toprak MS, Soliman HMA, Zhou J, Muhammed M, Platzek D, Muller E (2006) Chem Mater 18:3627
39. Richoux V, Diliberto S, Boulanger C, Lecuire JM (2007) Electrochim Acta 52:3053
40. Wang W-L, Wan C-C, Wang Y-Y (2007) Electrochim Acta 52:6502
41. Zimmer A, Stein N, Johann L, Beck R, Boulanger C (2007) Electrochim Acta 52:4760
42. Li S, Soliman HMA, Zhou J, Toprak MS, Muhammed M, Platzek D, Ziolkowski P, Müller E (2008) Chem Mater 20:4403
43. Ham S, Jeon S, Lee U, Park M, Paeng KJ, Myung N, Rajeshwar K (2008) Anal Chem 80(17):6724
44. Diliberto S, Richoux V, Stein N, Boulanger C (2008) Phys Status Solidi 205:2340
45. Glatz W, Durrer L, Schwyter E, Hierold C (2008) Electrochim Acta 54(2):755
46. Chen CL, Chen YY, Lin SJ, Ho JC, Lee PC, Chen CD, Harutyunyan SR (2010) J Phys Chem C 114:3385
47. Ma Y, Johansson A, Ahlberg E, Palmqvist AEC (2010) Electrochim Acta 55:4610
48. Ma Y, Ahlberg E, Sun Y, Iversen BB, Palmqvist AEC (2011) Electrochim Acta 56:4216
49. Soliman HMA, Kashyout AHB (2011) Engineering 3:659
50. Erdogan IY, Demir U (2011) Electrochim Acta 56(5):2385

51. Li W-J (2009) Electrochim Acta 54:7167
52. Nguyen HP, Wu M, Su J, Vullers RJM, Vereecken PM, Fransaer J (2012) Electrochim Acta 68:9
53. Li W-J, Yu W-L, Yen C-Y (2011) Electrochim Acta 58:510
54. Fung YS, Zhang WB (1997) J Appl Electrochem 27(7):857
55. Pan G-B, Freyland W (2007) Electrochim Acta 52(25):7254
56. Fu Y-C, Su Y-Z, Zhang H-M, Yan J-W, Xie Z-X, Mao B-W (2010) Electrochim Acta 55:8105
57. Abbott AP, Ryder KS, Konig U (2008) Trans Inst Met Finish 86:196
58. Golgovici F, Cojocaru A, Nedelcu M, Visan T (2009) Chalcog Lett 6(8):323
59. Golgovici F, Cojocaru A, Agapescu C, Jin Y, Nedelcu M, Wang W, Visan T (2009) Studia Univ Babes Bolyai Chemia 54(1):175
60. Golgovici F, Cojocaru A, Nedelcu M, Visan T (2010) J Electron Mater 39(9):2079
61. Golgovici F, Cojocaru A, Anicai L, Visan T (2011) Mater Chem Phys 126:700
62. Abbott AP, Boothby D, Capper G, Davies DL, Rasheed RK (2004) J Am Chem Soc 126:9142
63. Chaouni H, Bessieres J, Modaressi A, Heizmann JJ (2000) J Appl Electrochem 30(4):419